УДК 551.243:551.3.051:004:925.8

В. ФЬЕЛДСКААР (Тектонор, Ставангер, Норвегия),
Э. АНДЕРСЕН, Х. ИОХАНСЕН (Айрис, Ставангер; Верико, Ставангер, Норвегия),
Р. ЛАНДЕР (Айрис, Ставангер, Норвегия; Геокосм, Дюранго, Колорадо, США),
В. БЛОМВИК (Айрис, Ставангер; Верико, Ставангер, Норвегия),
О. СКУРВЕ (Айрис, Ставангер, Норвегия),
Д. К. МИХЕЛЬСЕН (Айрис, Ставангер, Норвегия; Гигавиз, Тулза, Оклахома, США),
И. ГРЮННАЛЕЙТЕ (Тектонор, Ставангер, Норвегия), Д. МЮККЕЛТВЕЙТ (Айрис, Ставангер, Норвегия)

Преодоление проблем моделирования бассейнов с учетом структурной геологии

Модели бассейнов реконструируют временную, пространственную и физическую эволюцию свойств осадочных бассейнов и являются важным средством для прогнозирования возникновения и свойств накоплений углеводородов. Хотя многие ловушки углеводородов связаны со сложными геологическими структурами, большинство современных систем моделирования бассейнов значительно упрощает их геометрические реконструкции. В статье описываются три метода повышения эффективности моделирования бассейна в структурно сложных регионах:

1) геометрическая реконструкция взаимосвязанных массивов с разломами сбросового и взбросового типа;

2) геометрическая реконструкция солевых структур;

3) моделирование теплового потока, связанного с магматическими интрузиями.

Каждый метод значительно улучшает точность ввода данных для теплового моделирования (а также потенциально для моделирования потоков флюидов).

Методы улучшенной геометрической реконструкции упрощают результаты моделирования бассейна в основном за счет более реалистичных пространственных реконструкций слоев и сопряженных свойств горных пород. Модели опускания/поднятия обеспечивают более точные реконструкции теплового потока, а также полезны для оценки вероятных глубин залежей флюидов. Моделирование диагенеза песчаника обеспечивает улучшенную точность для прогнозирования свойств пород, таких как пористость, проницаемость и теплопроводность, и более реалистичное моделирование интервального уплотнения и соответствующего проседания.

Ключевые слова: *моделирование бассейна, разрушение, соль, уплотнение, диагенез песчаника.*

W. FJELDSKAAR (Tectonor AS, Stavanger, Norway),
Å. ANDERSEN, H. JOHANSEN (IRIS, Verico, Stavanger, Norway),
R. LANDER (IRIS, Stavanger, Norway; Geocosm LLC, Durango, Colorado, USA),
V. BLOMVIK (IRIS, Verico, Stavanger, Norway),
O. SKURVE (IRIS, Stavanger, Norway),
J. K. MICHELSEN (IRIS, Stavanger, Norway; Gigawiz Ltd Co, Tulsa, Oklahoma, USA),
I. GRUNNALEITE (Tectonor AS, Stavanger, Norway), J. MYKKELTVEIT (IRIS, Stavanger, Norway)

Bridging the gap between basin modelling and structural geology

Basin models reconstruct the temporal, spatial, and physical property evolution of sedimentary basins and are important means for predicting the occurrence and properties of hydrocarbon accumulations. While many hydrocarbon accumulations are associated with complex geological structures, most basin modelling systems greatly oversimplify the geometric evolution of such structures. This paper describes three methods for improving basin modelling performance in structurally complex regions:

(1) geometric reconstruction of interconnected normal and reverse fault arrays,

(2) geometric reconstruction of salt structures, and

(3) simulation of heat flow associated with magmatic intrusions.

Each of these methods significantly improves the accuracy of input constraints for thermal simulations (as well as potentially for fluid flow simulations).

The geometric reconstruction methods improve basin modelling results mainly by allowing for more realistic representations of the spatial geometries of geologic strata and their associated rock properties. The subsidence / uplift models provide more accurate heat flow reconstructions and also are useful for estimating likely paleowater depths. The sandstone diagenesis modelling provides substantially improved accuracy for prediction of rock properties such as porosity, permeability, and thermal conductivity together with more realistic simulation of interval compaction and associated subsidence.

Keywords: *basin modelling, faulting, salt, compaction, sandstone diagenesis.*

© Фьелдскаар В., Андерсен Э., Иохансен Х., Ландер Р., Блемвик В., Скурве О., Михельсен Д. К., Грюнналейте И., Мюккелтвейт Д., 2017

Introduction. In many hydrocarbon-bearing provinces structural events are a first order control on the timing and spatial distribution of hydrocarbon generation in addition to influencing the migration and entrapment of hydrocarbons. Basin models have the potential to unravel the complex interactions between the development of large-scale geologic structures and hydrocarbon generation and migration. Most current basin modelling systems, however, reconstruct geologic structures crudely, if at all. We designed the research software system BMT™ (a trademark of Tectonor AS, Stavanger) to provide a more rigorous approach toward simulation of hydrocarbon systems in structurally complex settings. This is possible because BMT is a 2D system, and is thus able to do modelling on complex structures within a reasonable time. Sensitivity analyses could be very important in structurally complex settings, and BMT is well suited for that because of very low CPU time. Sensitivity analyses are not possible with 3D systems in structurally complex settings, as input of parameters to 3D systems is a very time consuming process, and CPU time is a significantly obstacle.

Pertinent features of the system include:

Representation of sequence stratigraphic geometries and lithofacies distributions at a high spatial and temporal resolution in two-dimensional cross sections.

- Structural reconstruction [8]
  - automated area balanced reconstruction of interconnected normal and reverse fault arrays by vertical simple shear,
  - user-specified evolution in salt structures.
- Sediment compaction
  - Rigorous simulation of sandstone diagenesis via coupled mechanical and chemical process models [12],
  - exponential or linear porosity/depth curves are used for each lithology.
- Subsidence/heat flow simulation
  - flexural-isostatic response of the lithosphere to sedimentation/erosion and extension [8],
  - tectonic response to lithospheric thinning, including the effect of depth of 'necking' [8],
  - tectonic subsidence/uplift caused by changes in intra plate stress [8, 10],
  - heat flow from crustal and subcrustal thinning [5, 6].
- Thermal modelling
  - transient thermal modelling that considers advection of heat associated with faulting,
  - thermal effects of magmatic sills and underplating [5, 6],
  - hydrocarbon generation and oil-to-gas cracking [5].

BMT modelling involves the following steps: (1) definition of stratigraphic, structural, and depositional geometries in the present-day geologic section; (2) "backstripping" including sediment decompaction, automated fault restoration, user defined changes to salt geometry, and user definition of the geometry and lithologies for intervals that were eroded, if any; (3) forward modelling of section geometry to account for the influence of erosion and salt movement on sediment compaction and interval thicknesses; (4) forward simulation of isostatic and tectonic subsidence and uplift and associated heat flow using basin loading results derived from step 3; (5) forward transient thermal simulation that accounts for vertical and lateral mass and energy movements using reconstructed basin geometry from step 3 and basement heat flow from step 4; (6) simulation of hydrocarbon generation and oil-to-gas cracking using the temperature reconstructions from step 5, and (7) simulation of sandstone compaction and quartz cementation using the temperature reconstructions from step 5.

BMT is designed to represent unusually high degrees of geologic complexity with respect to structural features, stratigraphy, and lithologic distributions (Fig. 1). Incorporation of this complexity is possible due to a unique approach involving several separate gridding systems that have been optimized for accuracy and numerical efficiency. BMT gridding schemes include: (i) a polygon grid based on interpreted seismic sections that is used to represent the present-day geometry of depositional, hiatal, and erosional surfaces together with lithologic boundaries and fault surfaces, (ii) a "Bambino" grid based on the polygon grid that is used for reconstructing the geometry of the modelled region and that serves as a storage datum for rock properties and model results, (iii) a coarser vertical grid used for subsidence simulations and (iv) a high-resolution orthogonal grid used for thermal modelling.

Input Geology. The present-day geology of the modelled cross section is represented by digitized line segments that, in turn, are derived from seismic data. There are three line types used for this purpose (Fig. 2): "Timelines" represent depositional, hiatal, and erosional surfaces; "Faultlines" are used to represent interconnected arrays of normal and reverse faults; and "Litholines" define lithologic boundaries that occur within stratigraphic intervals. Lithologies are also assigned to polygons and serve as the basis for determination of various rock properties such as porosity, thermal conductivity, heat capacity, and source rock kinetics.

When the geometry of the various line types has been completely defined, BMT creates an interconnected set of polygons that are the basis for the "Bambino" grid discussed below. These polygons are the building blocks that BMT uses when it applies time-to-depth conversions, detects surfaces of erosion or non-deposition, and simulates sediment compaction and structural deformation.

BMT detects erosion when an older timeline is truncated by a younger one, forming an angular unconformity. BMT will not allow the user to proceed with the reconstruction process until the nature of the eroded interval is fully defined (Figs 3 and 4). The eroded interval will be reconstructed at the timeline when the erosion occurred.

"Bambino Grid". The "Bambino Grid" provides the basis for reconstruction of the cross section geometry in addition to serving as a data storage reference. Bambinos are vertical line segments that are connected to the base of a polygon (Fig. 5). They are created when a stratum is deposited and exist in all reconstructed timesteps younger than the depositional age of their host time-stratigraphic unit. The top of a Bambino is always at the line segment defining the top of its host polygon, and the length of the Bambino thus represents the thickness of the stratum at any particular time (Fig. 5). Bambinos refer to their host polygon to derive properties such as seismic velocity and lithology designation.

Bambinos within the same polygon maintain the same horizontal distance to their neighbors throughout

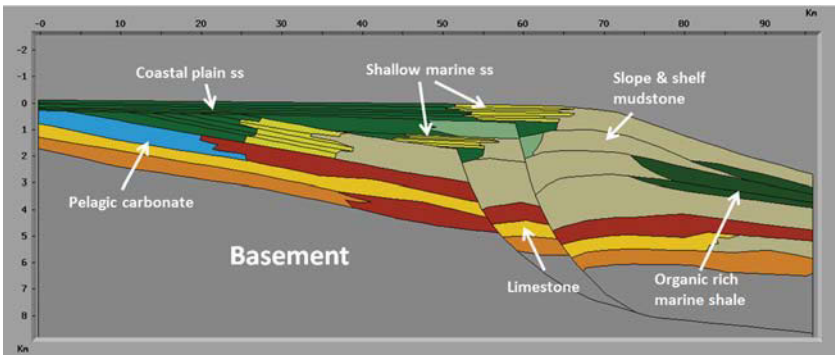

Fig. 1. BMT model in sequence stratigraphic environment

Рис. 1. Модель BMT в сейсмостратиграфической среде

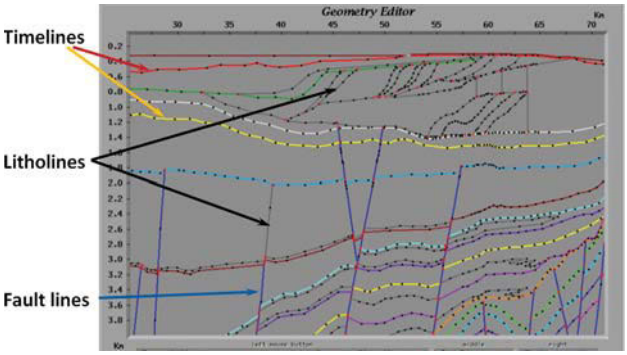

Fig. 2. Different line types defined in BMT; litholines, time lines and fault lines. The dots are the digital points

Рис. 2. Различные типы линий, определенные в BMT; литологические линии, линии времени и линии разломов. Данные точки являются цифровыми

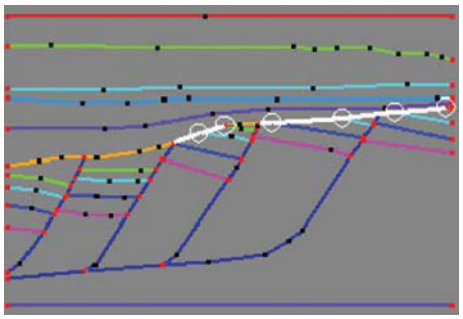

Fig. 3. BMT detects erosion (white lines) when an older timeline is truncated by a younger one

Рис. 3. BMT обнаруживает эрозию (белые линии), когда более ранняя линия времени усекается более поздней

Fig. 4. User-defined eroded timelines or faults. Left: BMT detects erosion surface when older timelines are truncated by a younger one. In this case several timelines have been eroded. Right: the nature of the eroded interval is fully defined

Рис. 4. Определенные пользователем временные линии или разломы, подвергшиеся эрозии. Слева: посредством системы BMT выявляются эрозионные поверхности, когда более поздние линии усекаются более ранней. В данном случае несколько временных линий подверглись эрозии. Справа: характер эродированного интервала определен полностью

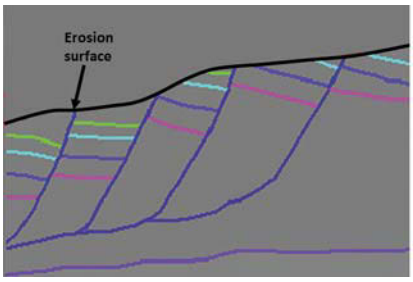

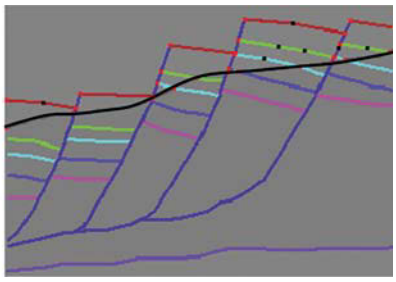

the reconstruction. If a strata polygon is cut by a fault, however, Bambinos in the hanging wall portion of the fault are translated with respect to footwall Bambinos according to the scheme described below (Fig. 6). Thus fault Bambinos are cut into two parts and the displacement of these parts marks the fault movement that has occurred between some time in the past and the present.

A Bambino is always created at each digitized point in the present-day polygon grid. Additional Bambino columns are added to the section automatically. The number of inserted Bambinos can be controlled by the user (the default is 70). These inserted columns are aligned vertically throughout the whole section at the top timestep, but will be offset at fault boundaries after fault restoration. Bambinos store the following information:

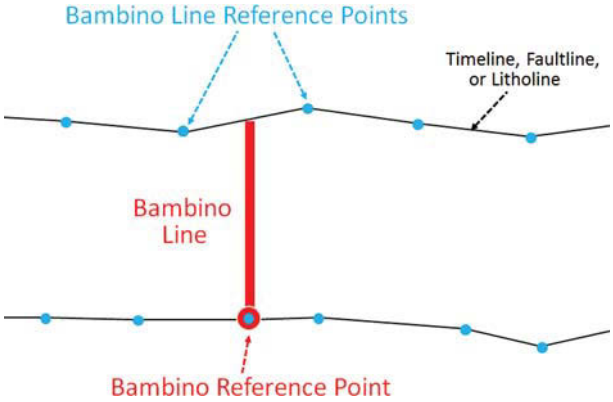

Fig. 5. Illustration of reference points that define the Bambino Lines

Рис. 5. Иллюстрирование опорных точек, определяющих линии Bambino (отрезки вертикальной линии, которые соединены с основанием полигона)

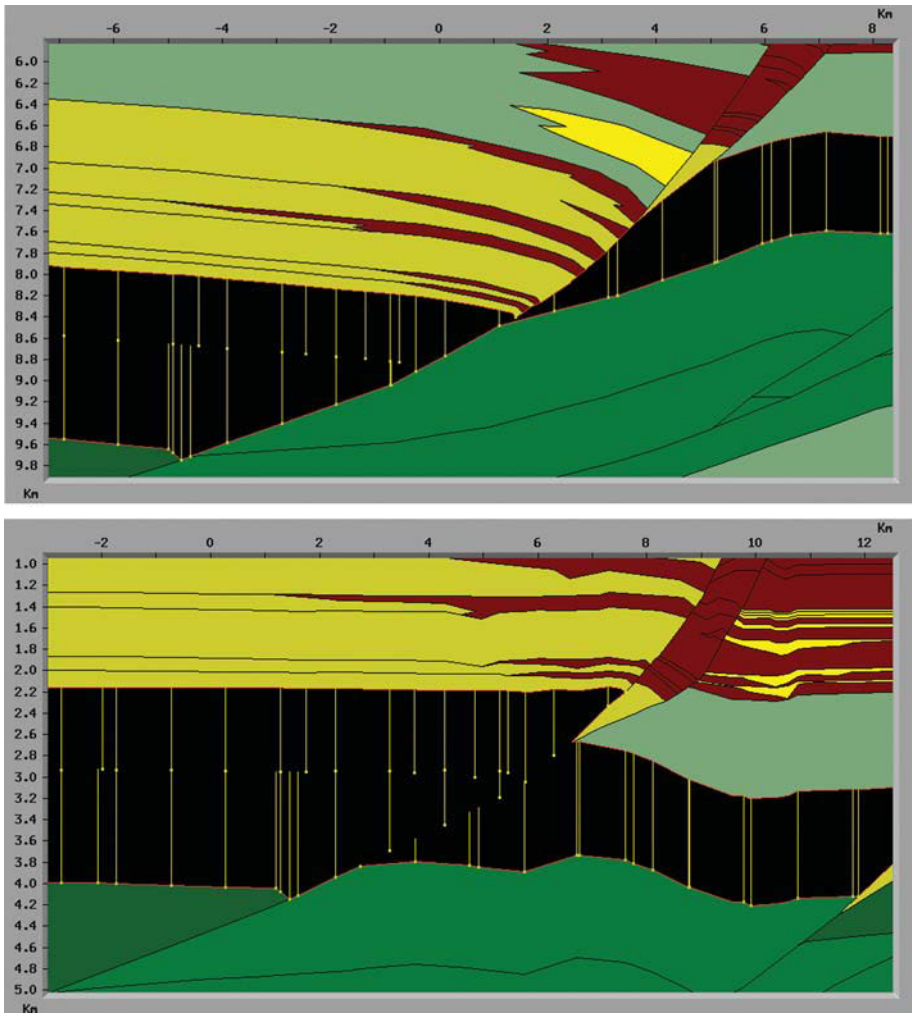

Fig. 6. Example of the Bambino Grid present timestep (upper figure) and at a reconstructed timestep (lower figure). If a strata polygon is cut by a fault, Bambinos in the hanging wall portion of the fault are translated with respect to footwall Bambinos. This is shown in the black formation

Рис. 6. Пример временного шага сетки Bambino, существующего на данный момент (сверху), и реконструированного временного шага (снизу). Если полигон напластований разрезан разломом, Bambinos в части висячего бока разлома перемещаются в соответствии с лежачим боком Bambinos. Это показано в черной части рисунка

- the Bambino reference point and Bambino line reference points (as shown in Fig. 2 the reference point is the point on the lower Polygon Line segment to which the Bambino is attached, and the Line reference points are two points on the upper line segment of the Polygon that straddle the Bambino),
- the x and z coordinates of the Bambino reference point for each reconstructed timestep,
- the maximum burial depth yet encountered for the Bambino reference point at each reconstructed timestep,
- the Bambino line length for every reconstructed timestep,
- temperature and maturation data.

Geohistory Reconstruction. The first step in the reconstruction at a particular timestep is to remove the top layer, and decompact the remaining layers using porosity depth functions. Next all the faults that intersect the new top surface are restored. Finally the elevation of the top surface is adjusted using the user defined paleowater depth as a datum.

Sediment Decompaction is based on porosity-depth trends for each defined lithology and the thickness of overlying sediments (e.g. [13]). The mean porosity φ for a Bambino line with top z_1 and bottom z_2 is

$$\phi = \frac{\phi_0}{c}\frac{e^{-cz_1} - e^{-cz_2}}{z_1 - z_2},$$

where φ is porosity (fraction), φ_0 is the surface porosity (fraction), c is a constant in km^{-1} and z is the depth in km.

When the top of the Bambino line moves from z_1 to z'_1, the new bottom position z'_2 is calculated using the following expression

$$z'_2 + \frac{\phi_0}{c}e^{-cz'_2} + \frac{\phi_0}{c}e^{-cz_2}\left(e^{-cz_1} - e^{-cz_2} - e^{-z_1}\right) + z_1 - z_2 - z'_1 = 0.$$

This expression is solved numerically for z'_2 using Newton's Method.

Fault Restoration is included in BMT to account for structural effects on temperature and maturation

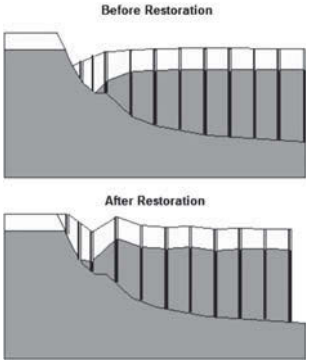

Fig. 7. Illustration of vertical shear method for fault restoration

Рис. 7. Иллюстрирование метода вертикального сдвига для восстановления разлома

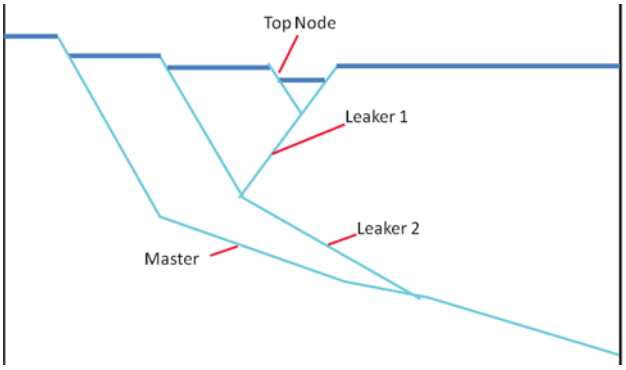

Fig. 8. An example of the fault types defined by BMT's restoration algorithm

Рис. 8. Пример видов разломов, выявленных с помощью алгоритма восстановления BMT

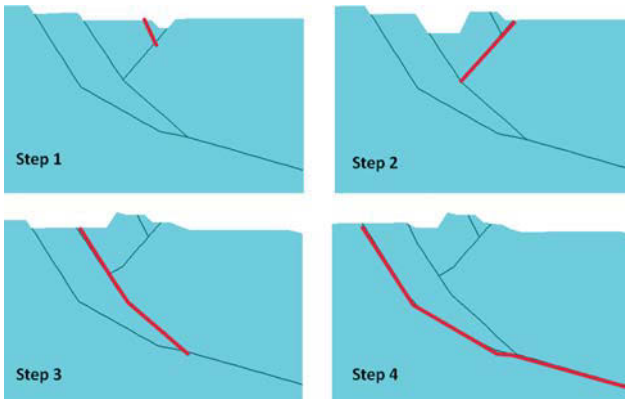

Fig. 9. Illustration of the sequence of restoration steps taken in a fault complex. Upper left figure is the present day situation. The steps are: 1) restore Top Node; 2) restore Leaker1; 3) restore Leaker2; 4) restore Master

Рис. 9. Иллюстрирование последовательности этапов восстановления, предпринятых в комплексе разломов. Верхний слева рисунок отображает современную ситуацию. Этапы: 1) восстановление Top Node; 2) восстановление Leaker1; 3) восстановление Leaker2; 4) восстановление Master

timing and to give insights into the geometry of possible hydrocarbon migration pathways and traps through time. Many workers have presented geometric and physical models of hanging-wall collapse along vertical or steeply dipping shear surfaces (e.g., [9, 18]).

There are a number of fault restoration methods described in the literature such as vertical shear, inclined shear, bedding plane slip, slip line, etc. Dula (1991) [3] provides a review of these and discusses how the methods compare with clay models and seismic data. In general, Dula found that the inclined shear model with an antithetic shear of 20° gave the best fit with observations although all models did a reasonably good job of restoration. The vertical shear method also gave very good results.

Requirements for temperature and maturation modelling impose some restrictions on the way that BMT restores faults compared to other specialized fault restoration programs. In such programs, fault blocks are permitted to have gaps or overlaps during restoration to datum surfaces. BMT, however, requires a continuous geological section for temperature and maturation modelling. Gaps in the section cannot be tolerated by the system because they are discontinuities to transfer of heat. Overlaps also cannot be tolerated because the ambiguity that arises for defining the thermal properties of the system for a given point in the overlap zone. Thus BMT uses the vertical shear method for fault restoration because it provides a good approximation to observed fault displacements, can track rock mass, and needs less user interaction than the inclined shear method which requires that shear angles be defined on a fault-by-fault basis.

An example of a BMT fault restoration is shown for a listric growth fault in Fig. 7. For the sake of simplicity, the figure does not show how the system accounts for the effects of compaction and maintains area balance. During the reconstruction, the vertical bars are translated up the fault system until the top surface is continuous across the fault. The lateral translation, which is significant, is shown by the gap on the right hand side of the restored portion of Fig. 7. This restoration method is called vertical shear because the bars remain vertical throughout the fault restoration process. In our implementation of vertical shear the hanging wall portion of the fault block is draped over the fault surface after it is moved (Fig. 7), and results in a deformation of the hanging wall part of the fault block. The vertical shear ensures that there is no overlap or gaps in the geologic section that could cause errors in the temperature and maturation simulations.

The steps taken to restore an individual fault segment are:

1. The restoration process begins by calculating the lateral distance, Δx, for the translation of the hanging wall portion of the fault block during reconstruction. This is done by measuring the lateral distance between the fault and its intersection with the hanging and footwall portions of the timeline to be restored.

2. The Bambino grid elements that are in the hanging wall portion of the fault and are attached to the fault plane must be given new reference points (ID) during the restoration. This step ensures that the movement of mass resulting from fault restoration is accounted for properly. The new Bambino reference positions are obtained by adding Δx to the pre-restoration ID and projecting the z coordinate onto the fault line at the new corresponding x position.

3. Restoration of faults that intersect the side boundaries of the model requires that new material is brought into the model area (Fig. 7). This new material is automatically given the same Δz as the reference point line that defines the point on the edge of the model before fault movement.

The system also reconstructs thrust faults if they can be represented by simple reverse fault geometries. In addition to restoring "single" faults such as the example

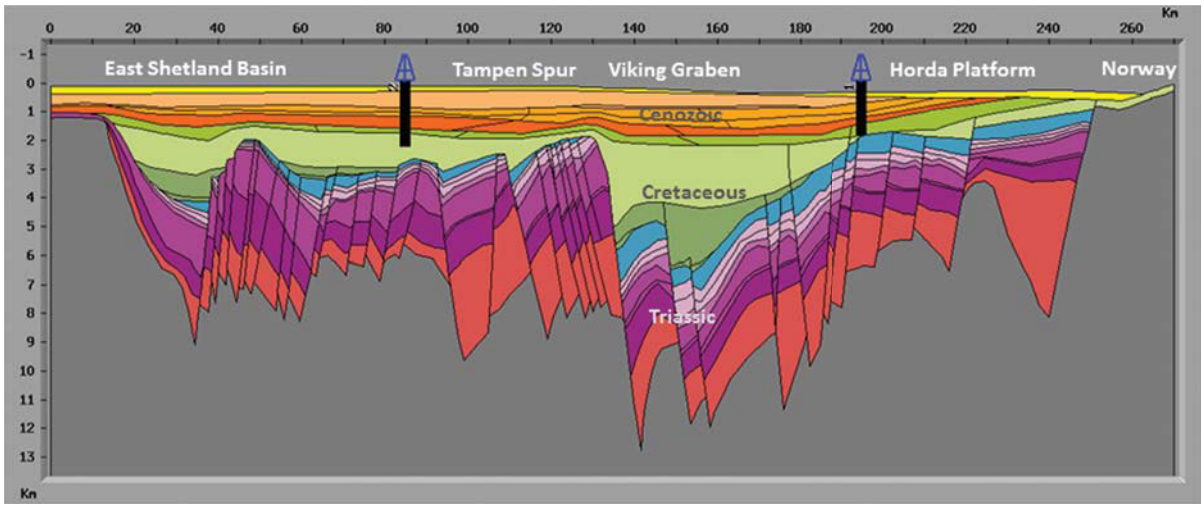

Fig. 10. Transect across the North Sea, with extensive faulting in the rift phase as is typical for an extensional basin. Display of two calibration wells (at 85 km and 195 km) are also shown

Рис. 10. Трансект через Северное море, характерный для вытянутого бассейна с обширной сбросовой деятельностью в фазе рифтинга. Также даны показания двух калибровочных скважин (на 85 и 195 км)

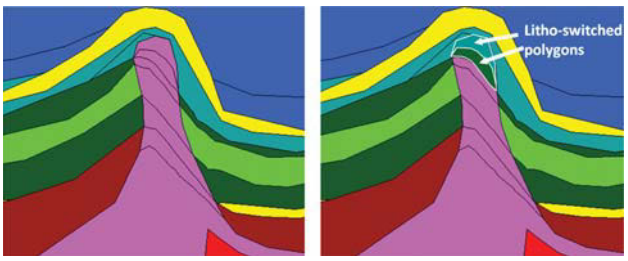

Fig. 11. Illustration of litho-switching in modelling of salt movements. The salt lithology for a polygon is changed at a given time

Рис. 11. Иллюстрация в моделировании лито-переключения движения солей. Литология солей для полигона изменяется в заданный момент времени

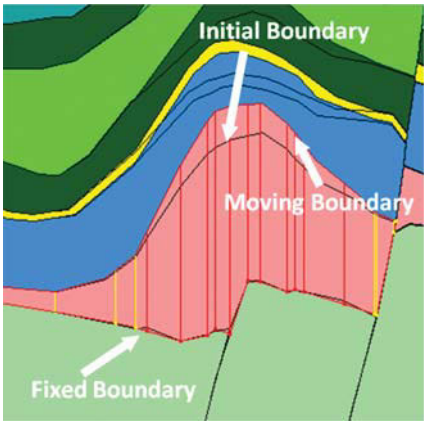

Fig. 12. Polygon inflation. The selected gridlines (red color) are extended above the upper (moving) boundary while remaining fixed along the lower boundary. Note how overlying polygons are pushed upwards

Рис. 12. Вздувание полигона. Отобранные линии сетки (красный цвет) выходят за нижнюю (движущуюся) границу, оставаясь неподвижными вдоль верхней границы. Обратите внимание на то, как нижележащие полигоны выталкиваются вниз

above, BMT also restores interconnected fault complexes by analyzing the hierarchy of constituent faults and systematically propagating displacement among them (Fig. 8). At the base of the hierarchy is the "master" fault, which receives the cumulative displacement from other higher level faults while passing none on to other faults. At the top of the hierarchy are "top node" faults that propagate displacement on other faults while receiving none. "Leaker" faults are intermediate in the hierarchy and both accept and propagate displacement from other faults. BMT uses this hierarchy to reconstruct each fault complex starting with the "top node", working progressively through each "leaker", and finally to the "master" (Fig. 9). Once all fault complexes have been restored the system determines the burial depth for each Bambino point by working downward from the upper boundary of the section. BMT then renders the restored section geometry given the user defined paleowater depth profile and the Bambino x and z locations and line lengths.

The ability of fault restoration for temperature calculations is particularly important in extensional settings (Fig. 10).

Salt Reconstruction. Salt structures are attractive targets for hydrocarbon exploration all over the world. The low density and the viscous nature of salt enable it to deform by buoyancy flow, deforming and perhaps penetrating sedimentary sequences above it. Hydrocarbons may be trapped under large salt domes, along salt flanks, or along salt associated faults. The structural traps as we see on present seismic sections are unlikely to be the structures that were in place when hydrocarbons migrated into the area. Thus reconstructing the evolution of salt structures may be crucial for constraining the filling and spilling of hydrocarbon accumulations. Because the high thermal conductivity of salt, salt structures act like heat pipes and can dramatically change subsurface temperatures, potentially affecting the timing of hydrocarbon maturation.

Simulating the evolution of a salt structure is not straightforward because many different processes and deformation mechanisms are involved. Salt deforms

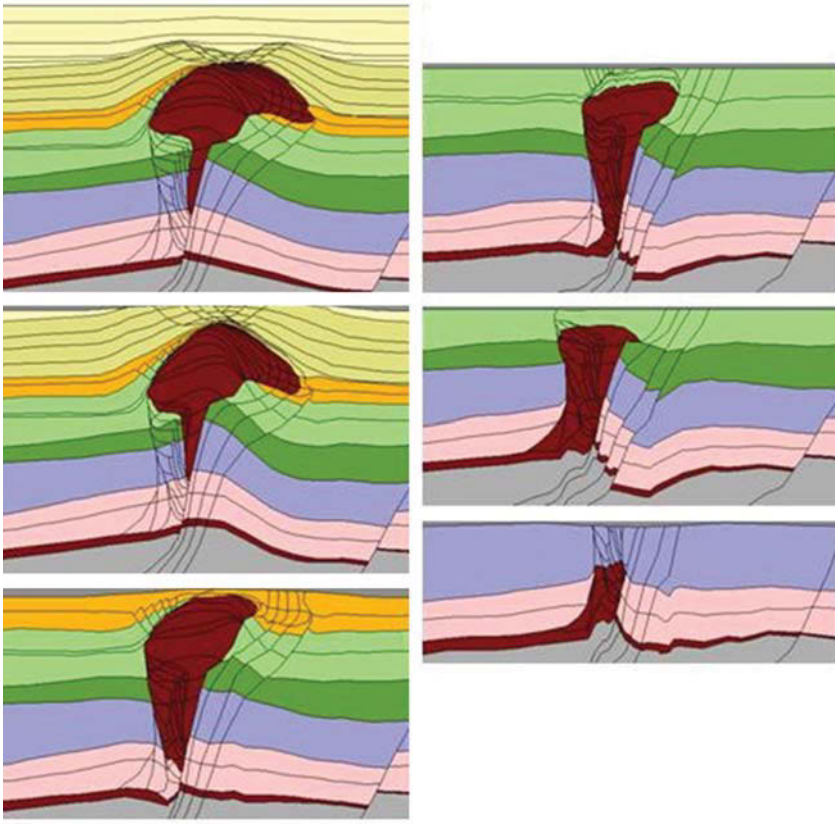

Fig. 13. Profile over a salt dome from the Central Graben, North Sea, with modelled evolution of the salt by litho-switching and inflation/deflation technique. The snapshots are for present day, 18, 38, 61, 75 and 130 Ma

Рис. 13. Профиль над соляным куполом из Центрального грабена (Северное море), вместе с моделируемым развитием солей с применением метода лито-переключения и приёмов спада/подъема. Снимки соответствуют ситуации на данный момент, 18, 38, 61, 75 и 130 млн лет

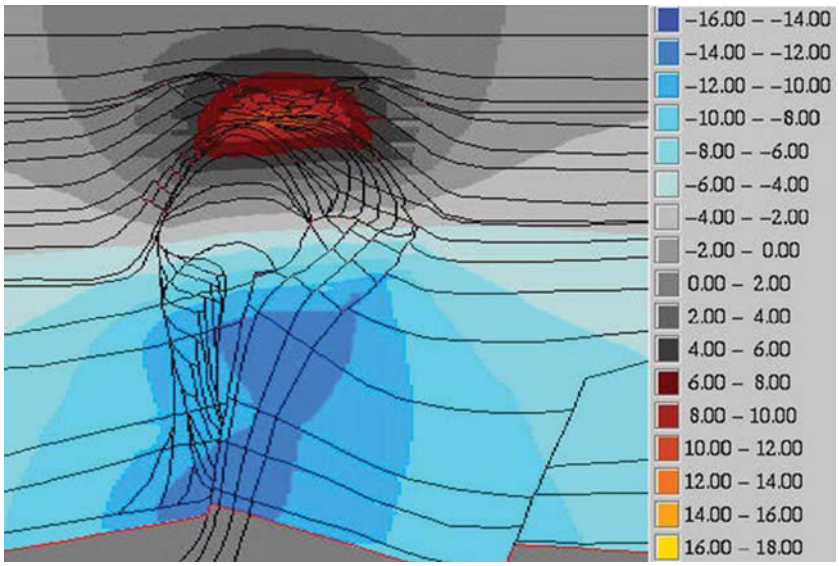

Fig. 14. Modelled temperature effect of the salt pillow of Figure 13. The figure shows the difference of the temperature field in (°C) calculated with salt lithology versus sediment lithology

Рис. 14. Моделируемый температурный эффект солевого купола рис. 13. Показана разница температурного поля в °C, вычисленного по литологии солей в сравнении с литологией отложений

as a viscous fluid, whereas the surrounding sediments typically deform by brittle and/or viscous and elastic mechanisms. Salt movement may be triggered by local faulting or regional extension or compression, differential loading, erosion, dissolution etc. [14], and the mobilization of the salt invoke several other processes that can reinforce the salt flowage. Salt flowage and accumulation of salt in central pillows, domes or diapirs assume withdrawal and thinning of the salt from the surrounding area (e.g. [16]). This again causes increased subsidence and collapse of the overburden, which provides accommodation space for sedimentation, in turn enhancing the salt drive. Likewise, doming and uplift of overburden above the evolving salt may lead to erosion, increasing the gravity instability by removing mass above the thickest part of the salt and loading erosive material on the flanks. The upward movement of salt will apply an upward force on the sedimentary overburden. This effect can create overpressure in certain areas and affect the sealing and fluid-flow properties of a reservoir.

In BMT salt movement is simulated during backstripping by manual editing of the salt geometry at every appropriate time step. Salt reconstruction is accomplished by: (1) changing the lithology of a polygon at a given time (litho-switching) and (2) inflating or deflating salt polygons. Litho-switching allows adding or removing portions of a salt body to mimic salt growth or withdrawal (Fig. 11). It is used when a salt body completely pierces overlying sediments or when the salt body thickens horizontally, for example. Inflation and deflation allows the size

and shape of a single salt polygon or a set of salt polygons to be changed (Fig. 12). A polygon is inflated or deflated by increasing or decreasing the length of the selected Bambino, which are connected along the upper and lower boundaries of a polygon. When a selected Bambino is inflated or deflated it will remain fixed with respect to one of these boundaries while moving the other boundary upwards or downwards. The polygons may be vertically inflated to many times their original height or deflated to a thickness of less than one meter.

The mass added or removed by litho-switching is not accounted for in BMT. For example, if the lithology of a polygon is switched from salt to shale during reconstruction, the added shale mass is not automatically deducted from elsewhere in the shale unit. In essence the mass in a polygon that has been litho-switched spontaneously appears or disappears. However, BMT calculates the area of selected polygons allowing the user to keep track of the area added or removed by litho-switching. The user thus has the option of modifying a lithology unit by inflation/deflation to account for mass that has been added or removed by litho-switching.

Fig. 13 shows a cross-section from the Central Graben of the North Sea where salt movement was simulated during backstripping by editing salt geometry at every time step. The use of litho-switching and inflation facilities made it possible to produce realistic salt geometries through geologic time as illustrated in Fig. 13. The thermal conductivity of the salt gives a clear thermal impact, shown in Fig. 14. The temperature will be higher above the salt and significantly lower beneath the salt pillow, compared to a situation with only sedimentary thermal properties.

Subsidence and Thermal Modelling. BMT provides forward models of both isostatic and tectonic subsidence that can be used to generate overall subsidence models for the modelled cross section. These forward subsidence simulations are constrained by requiring their sum to match the subsidence history generated from the geohistory reconstruction described above (cf. [8]). An important output from the subsidence modelling is the palaeo heatflow.

The isostatic subsidence results from the load of the sediments and seawater through time and is associated with deposition, erosion and faulting. The isostatic model simulates how the lithosphere supports load through flexure as well as by buoyancy [7]. An analogue for the lithosphere is a thin elastic plate overlying an inviscid substrate. The thin elastic plate is characterized by its flexural rigidity D, or equivalently by its effective elastic thickness (EET), which we believe represents the mechanically strong part of the lithosphere in a depth-averaged sense [2]. The elastic strength varies over time and space, probably mainly due to variations in heatflow and the age of the load.

The tectonic subsidence is a quantification of the effects of crustal and sub-crustal thinning, i.e. the subsidence an extensional basin would undergo if it was not loaded with sediments. BMT's forward model for the theoretical tectonic subsidence is a two-dimensional non-uniform extensional necking model, implying that the crustal thinning and the lithosphere heating do not necessarily have a one-to-one relationship [8]. The isostatic and tectonic models are based on a FFT algorithm [7], and use a gridding system consisting of equally spaced columns along the cross section. At each grid column the mass of the sedimentary section serves as an input parameter for subsidence calculations. The grid column positions are fixed throughout the simulation, but account for lateral movement of mass resulting from structural deformation.

Thermal Modelling Grid. The temperature calculation grid is a rectangular grid system suited for the application of finite difference calculations (Fig. 15). Thermal conductivity values used in the temperature calculation grid are derived from the Bambino grid. In most basin modelling systems the thermal grid geometry is tied to stratigraphic units. Such a gridding approach results in large-scale distortions to the grid geometry through geologic time due to depositional,

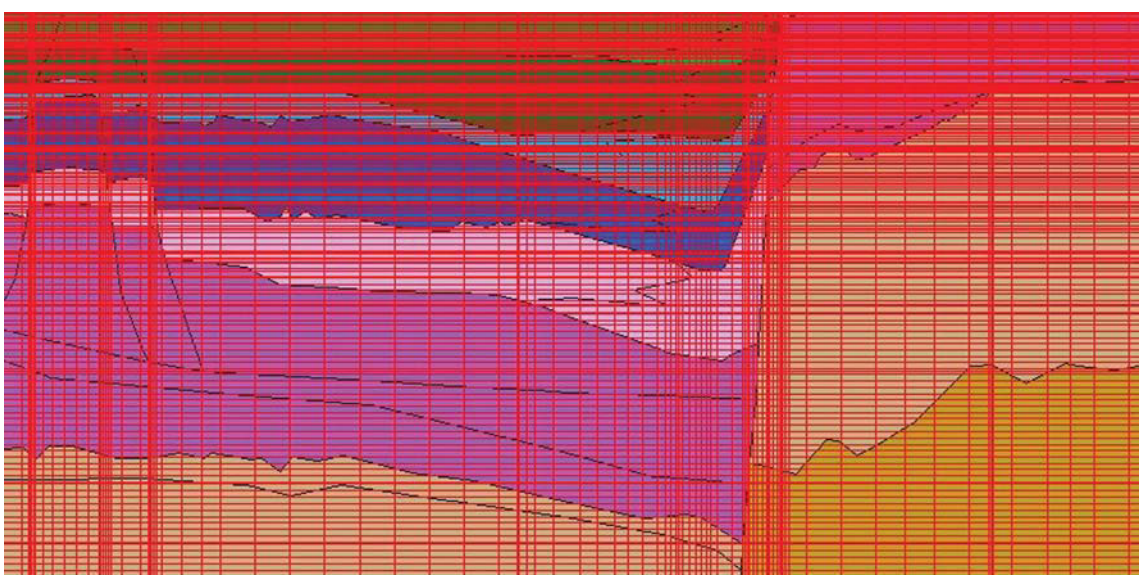

Fig. 15. Example of grid used for the temperature calculations. Horizontal and vertical grid lines are automatically inserted whenever needed for representing the geometry properly

Рис. 15. Пример сетки, используемой для расчета температур. Горизонтальные и вертикальные линии сетки автоматически вставляются всегда, когда это необходимо для правильного отображения геометрии

erosional and structural changes. By contrast, BMT creates a new high-resolution thermal modelling grid at each reconstructed timestep that represents spatial variations in rock properties at a high spatial resolution. In this way the thermal modelling grid always retains the orthogonal geometry that is required for accurate finite difference calculations.

Properties of the thermal modelling grid cells include heat capacities, vertical and horizontal thermal conductivities, and initial temperatures (from the previous timestep), and are derived from the Bambino lines. The porosity dependency of heat capacity and thermal conductivity are accounted for using the reconstructed porosities along the Bambino lines at each timestep. Grid cells intersecting Bambino lines directly derived their properties from the Bambinos (values are averaged when more than one Bambino intersects a cell). Cells not intersected by a Bambino line derive their properties by linear interpolation from the closest Bambinos.

A new, independent temperature calculation grid is made at each reconstructed timestep. The upper boundary condition for the thermal model is taken from a user-defined surface temperature that may vary through geologic time and across the modelled section. The lower boundary condition is defined by basement heat flow derived from the subsidence modelling (described above). The side boundaries are closed with respect to heat flow. Once the temperature has been calculated for a timestep it is extracted from the temperature calculation grid and stored on the Bambino grid. The temperature model is described in more detail in the Appendix.

The thermal conductivity values within the Bambino grid are determined using the porosity distribution along each Bambino and the linear porosity / conductivity function defined for the lithology of the Bambino. Vertical and horizontal thermal conductivity values from Bambinos are read into the nearest corresponding temperature calculation grid cell. Thermal conductivity values are averaged when more than one Bambino value occurs within a cell. Once the temperature has been calculated for a timestep it is extracted from the temperature calculation grid and stored on the Bambino Grid. The implemented temperature algorithm, described in more detail in the Appendix, is very efficient and ensures low CPU time even for unusually high temporal and spatial resolution. The thermal conductivity structure is one of the most important controls on its temperature distribution. The parameters that control the thermal conductivity structure are defined for each lithology type in the model, and BMT predicts the horizontal and vertical thermal conductivity of the lithology based on mineralogy and porosity of the sediments [4]. But there is anyway significant uncertainty in the resulting temperature. It is therefore important to calibrate the results with observed well data, which include present day temperature and vitrinite reflectance. BMT is flexible in its ability to simultaneously display model results and well-based measurements. Examples of calibration wells display are shown in Fig. 10.

Example Applications. A) *Fault restoration* method has been used in several basin modelling case studies on the Norwegian Continental Shelf as discussed above. We also have used BMT to reconstruct a cross section from the Gulf of Mexico basin with extensive listric faulting. The present-day geometry is shown in Figure 16a whereas Fig. 16b show two alternative reconstructions at 18.5 Ma (this corresponds to the upper portion of the second yellow unit from the top).

In the restoration that ignores fault reconstruction (Fig. 16b) the geometry of the footwall portions of fault blocks show geologically implausible geometries near the present-day location of fault "gaps" between stratigraphic surfaces. This geometry incorrectly implies a series of depositional hiatuses where the yellow unit is missing along the section such as from 4 to 5 km along the section where the orange unit is restored as being on the depositional surface instead of at ~2 km depth as shown in Fig. 16b. By contrast, BMT's fault algorithm was used to restore the fault complexes. The comparable sediment thicknesses across the faults left of 15 km along the section suggests that these faults formed after 18.5 Ma. The increase in thickness on the downthrown sides of faults to the right of 15 km along the section, however, suggests active growth faulting at this time. The reconstruction with simple vertical shear also indicates the substantial extension experienced by this section.

This systematic error in the reconstructed burial depth for the footwall portions of fault blocks results in substantial errors in temperature reconstructions. Fig. 16c shows the difference in simulated temperature at 18.5 Ma between the two alternative restoration models and indicates that the section lacking fault restoration has temperatures up to 80 °C lower than the structurally restored model due to errors in reconstructed burial depth in excess of ~2.5 km.

B) *Magmatism*. Magma transport often ends in or beneath extensional sedimentary basins. While it erupts at the surface, a significant part of the magma emplaces in depth as magmatic underplating trapped under the crust, or as basin forming sheet complexes dominated by horizontal sills associated with vertical dykes.

Magmatic underplating occurs when basaltic magmas are trapped during their rise to the surface at the Moho discontinuity or within the crust.

The magmatic underplating has two main effects. One is a short-lived (less than 5 m.y.) increase in heat flow related to dissipation of heat. The other is a longer-term effect associated with increased lithospheric stretching. The combined effects result in a heat pulse that will accelerate generation of oil and gas.

In the Vøring area offshore mid Norway there is a ''low-velocity layer'' observed on seismic refraction data. This low-velocity layer is termed the Lower Crustal Body (LCB). The thickness of LCB can exceed 8 km. Fjeldskaar et al. (2009) [5] studied the implications for the temperature regime and maturation historyfor a scenario where the LCB formed by magmatic underplating. The emplacement of the magmatic body was simulated by litho-switching from basement lithology to basaltic lithology with a starting temperature of 800–1100 °C. It was shown that the maximum temperature effects in the sediments was significantly (Fig. 17) and was achieved 2 million years after the underplating emplacement. More details in [5].

Magmatic sill intrusion. *Ma*ny extensional basins incorporate substantial volumes of saucer-shaped magmatic sills The sills are typically ~20–200 m thick with a lateral extent of ~10–20 km. When a large igneous event occurs, the emplacement of sill complexes may lead to substantial heating of the host sedimentary basin. Such thermal events may have important implications for organic matter maturation and rock diagenesis in sedimentary basins.

The emplacement of magmatic sills is simulated in BMT with the litho-switching technique. At the time

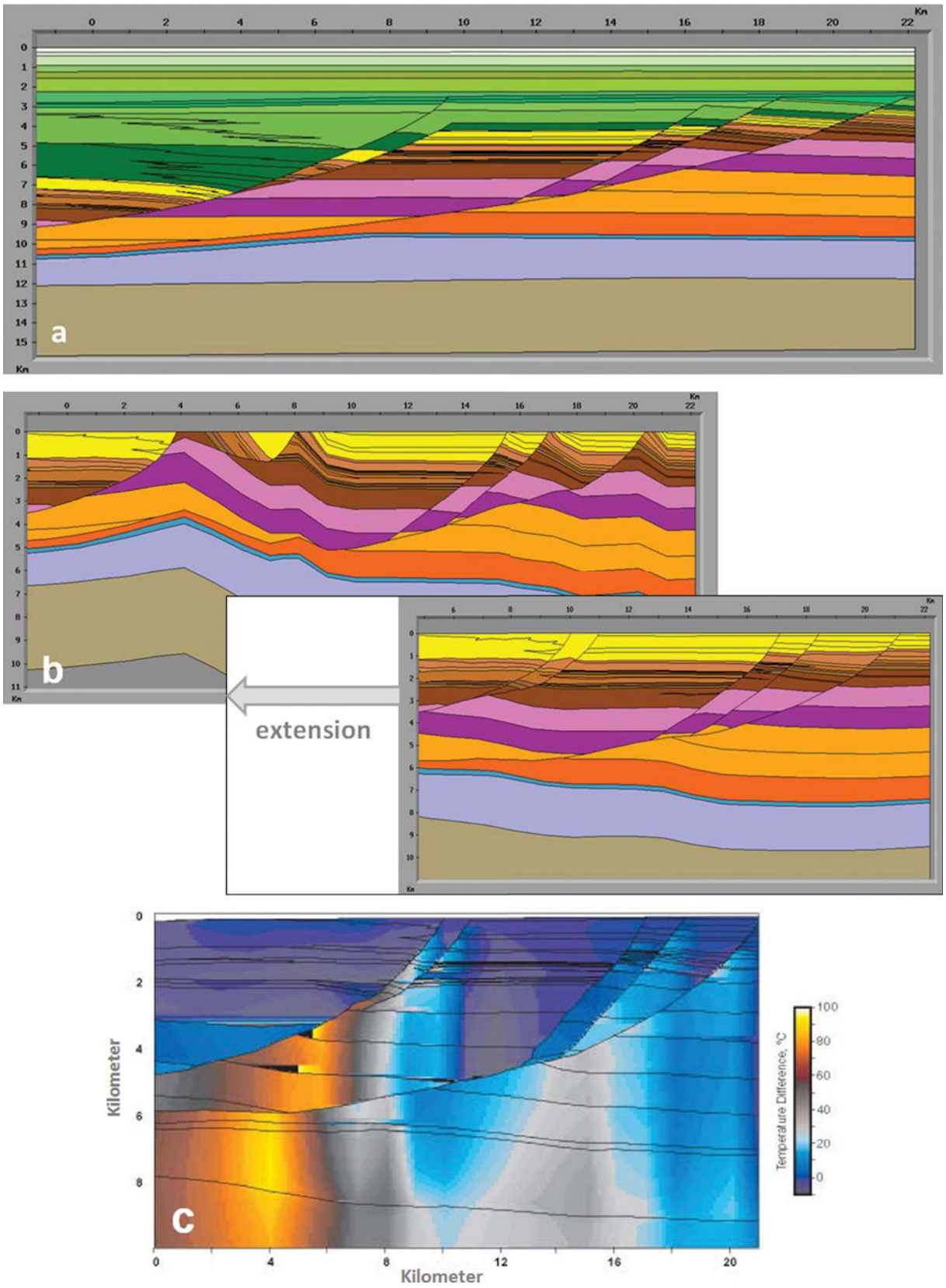

Fig. 16. a) 2D section from Gulf of Mexico with extensive listric faults. b) Example of reconstructed basin geometry using a simple 1D method (upper) and 2D listric fault model (lower). c) Temperature difference (in °C) between the two reconstruction methods; in this example close to 80 °C in the footwall portions of the profile

Рис. 16. a) Двухмерный разрез в Мексиканском заливе с обширными листрическими разломами. b) Пример реконструированной геометрии бассейна с использованием простого одномерного метода (верху) и модели двухмерного листрического разлома (внизу). c) Разность температур (в °C) между двумя методами реконструкции; в данном примере почти 80 °C на сегментах подошвы профиля

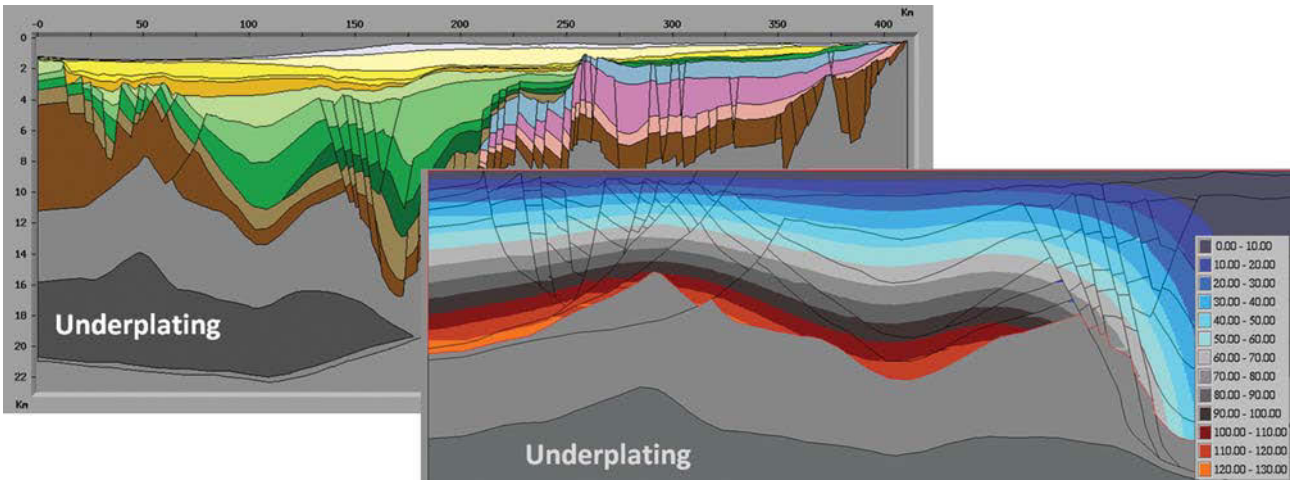

Fig. 17. A section over the Vøring area, offshore mid Norway with the mapped Lower Crustal Body at 16–18 km depth (left). The temperature effect of the possible magmatic underplating 2 million years after the emplacement is shown at the right

Рис. 17. Разрез по площади Вёринг, у побережья Центральной Норвегии, с нанесенными на карту низами земной коры (Lower Crustal Body) на глубине 16–18 км (слева). Справа показан температурный эффект возможного магматического подслаивания через 2 млн лет после внедрения

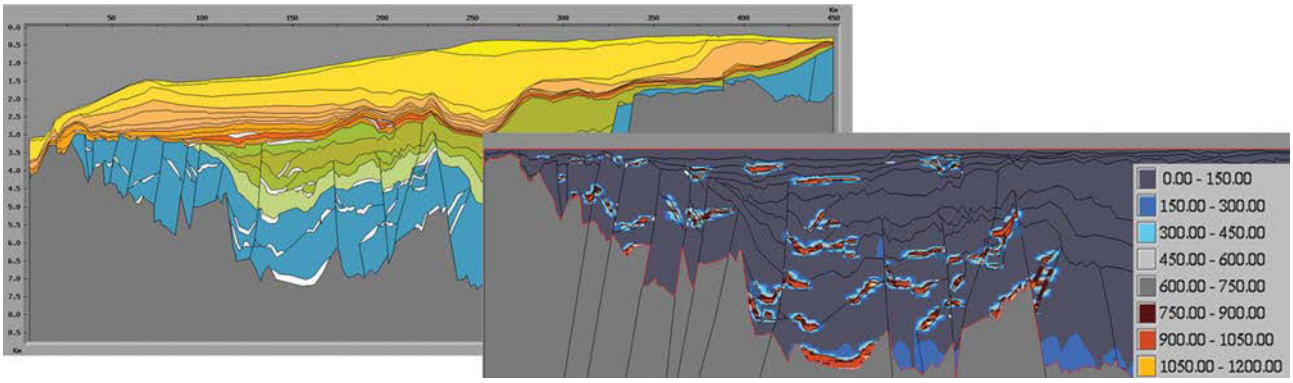

Fig. 18. Left: A section over the Vøring area (offshore mid Norway) with magmatic sill complexes (white polygons). Right: Modelled temperature effects (in °C) 100 years after the sill emplacement. The temperature of the sills is close to 1000 °C, but have started to cool, and the thermal anomalies will be smeared out over a large area and impact the generation of hydrocarbons over a large area (see [6] for more details)

Рис. 18. Разрез по площади Вёринг, у побережья Центральной Норвегии с комплексами магматического силла (белые полигоны). Моделируемые температурные эффекты через 100 лет после внедрения показаны на рисунке справа. Температура все еще близкая к 1000 °C, начнет понижаться, а аномалии теплового поля будут распространяться по большой площади и влиять на образование углеводородов на большой площади

of emplacement relevant polygons are switched from sediment lithology to basaltic lithology with starting temperature of 800–1100 °C. Figure 18 shows a modelled line from offshore mid Norway comprising of sill complexes [6]. The simulation of the temperature effects over time requires high spatial and temporal resolution as illustrated in Fig. 18, which shows the temperature effect 100 years after the sill emplacement. Over time the sills cool, and the temperature anomalies smear out over large areas. The thermal effects on the generation of hydrocarbons nonetheless can be very significant [6].

Conclusions. Basin models have the potential to unravel the complex interactions between the development of large-scale geologic structures and hydrocarbon generation and migration. Better insight into the mechanisms of basin formation has a direct bearing on the predictive power of basin models. We designed BMT to provide a rigorous approach toward simulation of hydrocarbon systems in structurally complex settings.

This paper presents three methods for improving basin modelling performance in structurally complex regions: (1) geometric reconstruction of interconnected normal and reverse fault arrays, (2) geometric reconstruction of salt structures, and (3) simulation of heat flow associated with magmatic underplating and magmatic sill intrusions. Each of these methods significantly improves the accuracy of input constraints for thermal simulations. The geometric reconstruction methods improve basin modelling results mainly by allowing for more realistic representations of the spatial geometries of geologic strata and their associated rock properties. Reconstructing the evolution of salt structures may be crucial for constraining the filling and spilling of hydrocarbon accumulations. The subsidence/uplift models provide more accurate heat flow reconstructions and

also are useful for estimating likely paleowater depths and basin structures.

We thank Lawrence Cathles and an anonymous referee for constructive comments on an earlier version of this paper.

APPENDIX. Numerical temperature model. The following equation are discretizised:

$$\partial/\partial x\, Kh\, \partial T/\partial x + \partial/\partial z\, Kv\, \partial T/\partial z = \partial/\partial t\,(cT),$$

where T is the temperature, Kh is the horizontal conductivity, and Kv is the vertical conductivity. Finite differences and a cell-centered grid are used. In the block with indices (ij) the expression

$$\partial/\partial z\, Kh\, \partial T/\partial z$$

is evaluated by the following formula [15]:

$$\left[\frac{\partial}{\partial x} Kh \frac{\partial T}{\partial x}\right] ij = \frac{1}{\delta x_i}\left[Kh_{i+1/2,j}\left(\frac{2\left(T_{i+1,j} - T_{i,j}\right)}{\delta x_i + \delta x_{i+1}}\right) - Kh_{i-1/2,j}\left(\frac{2\left(T_{i,j} - T_{i-1,j}\right)}{\delta x_{i-1} + \delta x_i}\right)\right]$$

$Kh_{i+1/2,j}$ is the value of Kh at the boundary between the blocks (i,j) and $(i+1,j)$. It is computed as the harmonic mean of $Kh_{i,j}$ and $Kh_{i+1,j}$. The expression $\partial/\partial z\, Kv\, \partial T/\partial z$ is treated analogously.

This gives $M \times N$ equations to find the $T_{i,j}$, unknowns, where $i = 1, 2, ..., M$ and $j = 1, 2, ..., N$. Here M and N are the number of blocks in x-direction and z-direction, respectively.

We use both Dirichlet and Neumann boundary conditions for the temperature model. For Dirichlet boundary conditions the temperature, T, at the boundary is given whereas for Neumann conditions the heat flux, $Kh\, \partial T/\partial z$ and $Kv\, \partial T/\partial z$, is given. A Neumann boundary condition with a heat flux of zero is used for the basin edges.

An iterative method is used to solve the linear system. Conjugate gradients are used as an acceleration method [11, 17]. The conjugate gradient method is preconditioned by nested factorization [1].

---

1. *Appleyard J.R., Cheshire I.M.* Nested factorization // Proceedings of the Seventh Symposium on Reservoir Simulation. Society of Petroleum Engineers of AIME, 1983. №12264. – P. 315–324.

2. *Burov E.B., Diament M.* The effective elastic thickness (Te) of continental lithosphere: What does it really mean? // J.G.R. 1995. Vol. 100. – P. 3905–3927.

3. *Dula J.W.F.* Geometric models of listric normal faults and rollover folds // AAPG Bull. 1991. Vol. 75. – P. 1609–1625.

4. *Fjeldskaar W., Christie O.H.J., Midttømme R.* et al. On the determination of thermal conductivity of sedimentary rocks and the significance for basin temperature history // Petroleum Geoscience. 2009. Vol. 15. P. 367–380, doi: 10.1144/1354-079309-814.

5. *Fjeldskaar W., Grunnaleite I., Zweigel J.* et al. Modelled palaeo temperature on Vøring, mid Norway – the effect of the Lower Crustal Body // Tectonophysics. 2009, doi:10.1016/j.tecto.2009.04.036.

6. *Fjeldskaar W., Helset H.M., Johansen H.* et al. Thermal modelling of magmatic intrusions in the Gjallar Ridge, Norwegian Sea: implications for vitrinite reflectance and hydrocarbon maturation // Basin Research. 2008. №20. – P. 143–159.

7. *Fjeldskaar W., Pallesen S.* The application of a viscoelastic lithosphere model to isostatic subsidence in backstripping / J. Collinson (Editor-in-Chief) // Correlation in Hydrocarbon Exploration. Graham and Trotman. Norwegian Petroleum Society, 1989. – P. 53–59.

8. *Fjeldskaar W., ter Voorde M., Johansen H.* et al. Numerical simulation of rifting in the northern Viking Graben: the mutual effect of modelling parameters // Tectonophysics. 2004. Vol. 382. – P. 189–212.

9. *Gibbs A.D.* Balanced cross-section construction from seismic sections in areas of extensional tectonics // J. of Structural Geology. 1983. Vol. 5. – P. 153–160.

10. *Grunnaleite I., Fjeldskaar W., Wilson J.* et al. Effect of local variations of vertical and horizontal stresses on the Cenozoic structuring of the mid-Norwegian shelf // Tectonophysics. 2009, doi:10.1016/ j.tecto.2009.01.005.

11. *Hageman L.A., Young D.M.* Applied iterative methods New York // Academic Press. 1981. – 386 p.

12. *Lander R.H., Walderhaug O.* Predicting porosity through simulating sandstone compaction and quartz cementation // AAPG Bull. 1999. Vol. 83. – P. 433–449.

13. *Sclater J.G., Christie P.A.F.* Continental stretching an explanation of the post-mid-cretaceous subsidence of the Central North Sea basin // J. of Geophysical Research. 1980. Vol. 85/B7. – P. 3711–3739.

14. *Stewart S.A., Clark J.A.* Impact of salt on the structure of the Central North Sea hydrocarbon fairways / A.J. Fleet, S.A.R. Boldy (eds.) // Petroleum geology of Northwest Europe: Proceedings of the 5th Conference. – London: Geological Society, 1999. – P. 179–200. Petroleum geology´86 Ltd.

15. *Thomas G.W.* Principles of hydrocarbon reservoir simulation. – Boston: International Human Resources Development Corporation (2nd ed.), 1982. – 207 p.

16. *Trusheim F.* Mechanism of salt migration in Northern Germany // Bulletin of the American Association of Petroleum Geologists. Vol. 44. №9. – P. 1519–1540.

17. *Young D.M., Jea K.C* Generalized conjugate acceleration of iterative methods, pt. 2: The nonsymmetrizable case // Report CNA-163: Center for Numerical Analyses. University of Texas at Austin, 1981. – 225 p.

18. *White N., Yielding G.* Calculating normal fault geometries at depth: theory and examples / A. Roberts, G. Yieldingand, B. Freeman (eds.) // The geometry of normal faulting. Geological Society of London Special Publication, 1991. № 56. P. 251–260.

---

1. Appleyard, J.R., Cheshire, I.M. 1983: Nested factorization: *Proceedings of the Seventh Symposium on Reservoir Simulation*, **12264**, 315–324. Society of Petroleum Engineers of AIME.

2. Burov, E.B., Diament, M. 1995: The effective elastic thickness (Te) of continental lithosphere: What does it really mean? *J.G.R. Vol. 100.* 3905–3927.

3. Dula, J.W.F. 1991: Geometric models of listric normal faults and rollover folds: *AAPG Bull., vol. 75.* 1609–1625.

4. Fjeldskaar, W., Christie, O.H.J., Midttømme, R., Virnovsky, G., Jensen, N.B., Lohne, A., Eide, G.I., Balling, N. 2009: On the determination of thermal conductivity of sedimentary rocks and the significance for basin temperature history. *Petroleum Geoscience. Vol. 15.* P. 367–380, doi:10.1144/1354-079309-814

5. Fjeldskaar, W., Grunnaleite, I., Zweigel, J., Mjelde, R., Faleide, J.I., Wilson, J. et al. 2009: Modelled palaeo temperature on Vøring, mid Norway – the effect of the Lower Crustal Body: *Tectonophysics*, doi:10.1016/j.tecto.2009.04.036.

6. Fjeldskaar, W., Helset, H.M., Johansen, H., Grunnaleite, I., Horstad, I. et al. 2008: Thermal modelling of magmatic intrusions in the Gjallar Ridge, Norwegian Sea: implications for vitrinite reflectance and hydrocarbon maturation. *Basin Research*, **20**, 143–159.

7. Fjeldskaar, W., Pallesen, S. 1989: The application of a viscoelastic lithosphere model to isostatic subsidence in backstripping. *In* Collinson, J. (Editor-in-Chief): *Correlation*

in Hydrocarbon Exploration. Norwegian Petroleum Society, Graham and Trotman, 53–59.

8. Fjeldskaar, W., ter Voorde, M., Johansen, H. et al. 2004: Numerical simulation of rifting in the northern Viking Graben: the mutual effect of modelling parameters. *Tectonophysics 382*, 189–212.

9. Gibbs A.D. 1983: Balanced cross-section construction from seismic sections in areas of extensional tectonics*: J. of Structural Geology, vol. 5.* 153–160.

10. Grunnaleite, I., Fjeldskaar, W., Wilson, J. et al. 2009: Effect of local variations of vertical and horizontal stresses on the Cenozoic structuring of the mid-Norwegian shelf: *Tectonophysics*, doi:10.1016/ j.tecto.2009.01.005.

11. Hageman, L.A., Young, D.M. 1981: Applied iterative methods New York: *Academic Press*. 386.

12. Lander, R.H., Walderhaug, O. 1999: Predicting porosity through simulating sandstone compaction and quartz cementation: *AAPG Bull., vol. 83.* 433–449.

13. Sclater, J.G., Christie, P.A.F. 1980: Continental stretching an explanation of the post-mid-cretaceous subsidence of the Central North Sea basin: *J. of Geophysical Research, vol. 85/ B7.* 3711–3739.

14. Stewart, S.A., Clark, J.A. 1999: Impact of salt on the structure of the Central North Sea hydrocarbon fairways. *In* Fleet, A.J. and Boldy, S.A.R. (eds.): *Petroleum geology of Northwest Europe: Proceedings of the 5th Conference,* 179–200. Petroleum geology´86 Ltd., Geological Society, London.

15. Thomas, G.W. 1982: Principles of hydrocarbon reservoir simulation. Boston, International Human Resources Development Corporation (2nd ed.), 207.

16. Trusheim, F. 1960: Mechanism of salt migration in Northern Germany: *Bulletin of the American Association of Petroleum Geologists*, *vol. 44*, 1519–1540.

17. Young, D.M., Jea, K.C. 1981: Generalized conjugate acceleration of iterative methods, pt. 2: The nonsymmetrizable case. *Report CNA-163: Center for Numerical Analyses*, University of Texas at Austin, 225.

18. White, N., Yielding, G. 1991: Calculating normal fault geometries at depth: theory and examples. *In* Roberts, A., Yielding, G. and Freeman, B. (eds.): *The geometry of normal faulting.* Geological Society of London Special Publication. **56**. 251–260.

Фьелдскаар Вилли – д-р философии, гл. науч. сотрудник, исслед. компания Тектонор (Норвегия), профессор, Ун-т Ставангера. Tectonor, c/o IPark, P.O. Box 8034, N-4068, Stavanger, Norway. <wf@tectonor.com>

Willy Fjeldskaar – Ph D, Chief Scientist, Tectonor AS, Stavanger, Norway. C/o IPark, P.O. Box 8034, N-4068, Stavanger, Norway. <wf@tectonor.com>

Åge Andersen – MSc, Engineer, Verico AS, Stavanger, Norway. <aage.andersen@verico.com>

Helge Johansen – MSc, Group leader, Verico AS, Stavanger, Norway. <helge.johansen@verico.com>

Robert H. Lander – Ph D, partner/scientific advisor, Geocosm LLC, Durango, Colorado, USA. <roblander@geocosm.net>

Vidar Blomvik – Software Engineer, Managing Director, Verico AS, Stavanger, Norway. <vidar.blomvik@verico.com>

Oddvar Skurve – MSc, retired. <skurv@online.no>

Johan K. Michelsen – MSc, CTO, Gigawiz Ltd Co, Tulsa, Oklahoma, USA. <jmichelsen@gigawiz.com>

Ivar Grunnaleite – Ph D, Structural geologist, Tectonor AS, Stavanger, Norway. <ig@tectonor.com>

Johannes Mykkeltveit – Dr. Philos., retired. <ingm-my@online.no>